^{236}Pu(n,f), ^{237}Pu(n,f), and ^{238}Pu(n,f) cross sections deduced from (p,t), (p,d), and (p,p') surrogate reactions

R. O. Hughes,[1,*] C. W. Beausang,[1] T. J. Ross,[1,†] J. T. Harke,[2] R. J. Casperson,[2] N. Cooper,[3] J. E. Escher,[2] K. Gell,[1] E. Good,[1] P. Humby,[3,‡] M. McCleskey,[4] A. Saastimoinen,[4] T. D. Tarlow,[1] and I. J. Thompson[2]

[1]*Department of Physics, University of Richmond, 28 Westhampton Way, Richmond, Virginia 23173, USA*

[2]*Lawrence Livermore National Laboratory, Livermore, California 94551, USA*

[3]*Wright Nuclear Structure Laboratory, Yale University, New Haven, Connecticut 06511, USA*

[4]*Cyclotron Institute, Texas A&M University, College Station, Texas, USA*

(Received 28 March 2014; revised manuscript received 28 May 2014; published 10 July 2014)

The ^{236}Pu(n,f), ^{237}Pu(n,f) and ^{238}Pu(n,f) cross sections have been inferred by utilizing the surrogate ratio method. Targets of ^{239}Pu and ^{235}U were bombarded with 28.5-MeV protons, and the light ion recoils, as well as fission fragments, were detected using the STARS detector array at the K150 Cyclotron at the Texas A&M cyclotron facility. The (p,tf) reaction on ^{239}Pu and ^{235}U targets was used to deduce the σ (^{236}Pu(n,f))/σ(^{232}U(n,f)) ratio, and the ^{236}Pu(n,f) cross section was subsequently determined for $E_n = 0.5$–7.5 MeV. Similarly, the (p,df) reaction on the same two targets was used to deduce the σ(^{237}Pu(n,f))/σ(^{233}U(n,f)) ratio, and the ^{237}Pu(n,f) cross section was extracted in the energy range $E_n = 0.5$–7 MeV. The ^{238}Pu(n,f) cross section was also deduced by utilizing the (p,p') reaction channel on the same targets. There is good agreement with the recent ENDF/B-VII.1 evaluated cross section data for ^{238}Pu(n,f) in the range $E_n = 0.5$–10.5 MeV and for ^{237}Pu(n,f) in the range $E_n = 0.5$–7 MeV; however, the ^{236}Pu(n,f) cross section deduced in the present work is higher than the evaluation between 2 and 7 MeV.

DOI: 10.1103/PhysRevC.90.014304 PACS number(s): 24.87.+y, 24.75.+i, 25.85.Ge, 25.55.Hp

I. INTRODUCTION

Present initiatives focusing on next-generation nuclear reactors, as well as ongoing stockpile stewardship needs, are driving interest in the measurement of neutron-induced fission cross sections for very short-lived actinide nuclei. Such cross sections are also important for constraining models for fission mechanisms that could be applicable to exotic heavy nuclei. However, by their very nature, producing the radioactive targets and high-neutron fluxes necessary to directly measure the cross sections of short-lived isotopes remains a major challenge.

In recent years the so-called surrogate method, originally pioneered by Cramer and Britt [1,2], has been utilized to measure numerous neutron-induced cross sections [3–18]. For (n,f) reactions, the extracted cross sections typically agree within 10% of established measurements. In the case of very short-lived isotopes, such surrogate reactions often provide the only practical means of deducing (n,f) cross sections by utilizing a stable beam and target combination. Recently [19], experiments utilizing (p,d) and (p,t) reactions as surrogates for (n,f) cross sections in uranium nuclei, where cross section data were previously well characterized, showed agreement with literature data within the experimental uncertainties of ∼9% and up to respective energies of ∼7 and ∼5.5 MeV. These results established the efficacy of such pickup reactions as surrogates for deducing (n,f) cross sections in the actinide region.

The present work utilizes (p,t), (p,d), and (p,p') surrogate reactions on a ^{239}Pu target to obtain cross sections for the ^{236}Pu(n,f), ^{237}Pu(n,f), and ^{238}Pu(n,f) reactions in a single experiment. The ^{238}Pu(n,f) cross section is well established both through direct (n,f) measurements and earlier surrogate reactions. The short half-lives for ^{236}Pu (2.8 years) and ^{237}Pu (46 days) make direct (n,f) cross section measurements experimentally challenging, and the (n,f) cross sections for these nuclei are ambiguous, as discussed below.

Figure 1(a) shows the available data for σ(^{237}Pu(n,f)). While there have been no direct (n,f) measurements, Britt and Wilhelmy used (^{3}He,xf) surrogate reactions to deduce σ(^{237}Pu(n,f)) in the range $E_n = 0.5$–6 MeV [20]. More recently, Younes, Britt, and Becker [21] re-analyzed the data of Britt and Wilhelmy. They employed updated nucleon-nucleus optical model potentials and introduced a correction to account for the spin mismatch between the neutron-induced and ^{3}He-induced reactions. The resulting (n,f) cross section is higher than the earlier results of Britt and Wilhelmy for energies below about 2 MeV. Above 2 MeV, the two data sets are in agreement (the uncertainties for the data of Britt and Wilhelmy were reported to be very small in Ref. [20]). The ENDF [22] and JENDL [23] data evaluations take into account only the data of Britt and Wilhelmy for this reaction cross section; however, as indicated by the figure, the ROSFOND [24] and CENDL [25] evaluations are inconsistent with the available data.

For the ^{236}Pu(n,f) cross section shown in Fig. 1(b), limited data are available from work by Vorotnikov *et al.* [26] and Gromova *et al.* [27] (these two works apparently use the

*Present address: Lawrence Livermore National Laboratory, Livermore, California 94551, USA.

†Present address: Department of Chemistry, University of Kentucky, Lexington, Kentucky 40506, USA.

‡Present address: Department of Physics, University of Richmond, 28 Westhampton Way, Richmond, Virginia 23173, USA.

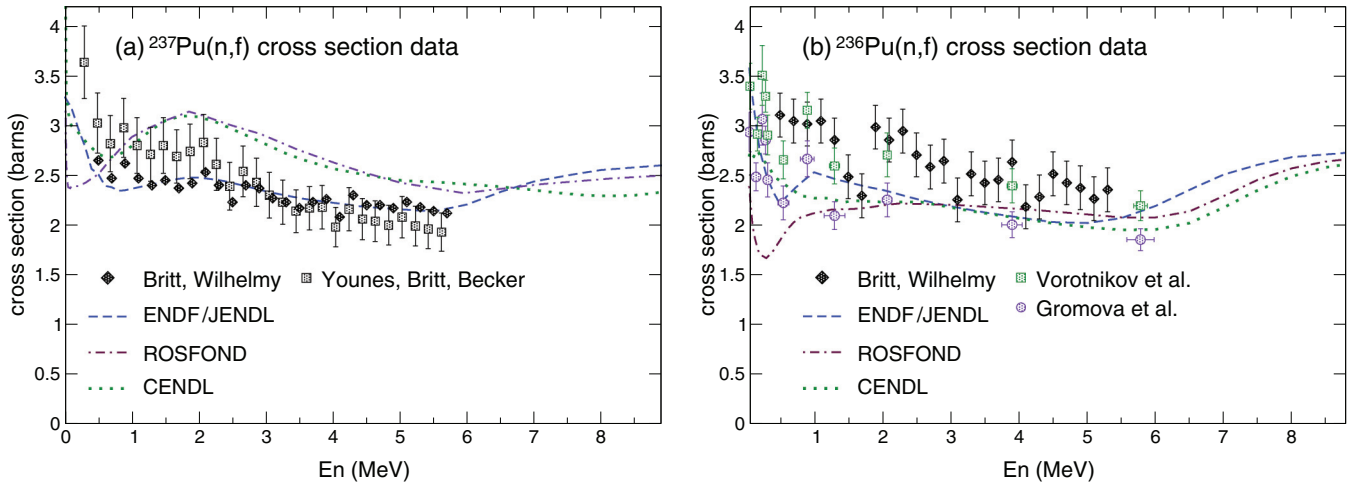

FIG. 1. (Color online) Experimental and evaluated cross section data for (a) $\sigma(^{237}\mathrm{Pu}(n,f))$ and (b) $\sigma(^{236}\mathrm{Pu}(n,f))$.

same data but with a shift in cross section of ∼0.5 barn on each point). Surrogate work by Britt and Wilhelmy are also available for this reaction [20]. It is apparent that the various data and evaluations for $\sigma(^{236}\mathrm{Pu}(n,f))$ disagree by up to one barn between 0 and 6 MeV.

II. THE SURROGATE METHOD

The surrogate method assumes that the cross section of a neutron-induced fission reaction, $\sigma_{(n,f)}$, can be separated into a compound nucleus (CN) formation cross section, σ_n^{CN}, and a fission decay probability, G_f^{CN}, according to Hauser-Feshbach formalism [28]:

$$\sigma_{(n,f)}(E_n) = \sum_{J^\pi} \sigma_n^{\mathrm{CN}}(E_n) G_f^{\mathrm{CN}}(E_n, J, \pi) \qquad (1)$$

The CN formation cross section is typically calculated while G_f^{CN} is deduced in the surrogate experiment. In the Weisskopf-Ewing approximation [29], the individual decay probabilities, $G_f^{\mathrm{CN}}(E_n, J, \pi)$, are assumed to depend only on the excitation energy of the decaying state and not on the spin and parity. In this case the exit channel $G_f^{\mathrm{CN}}(E_n)$ is independent of the entrance channel so that the surrogate reaction should yield the same fission decay probability as the direct (n,f) reaction.

In a surrogate measurement, the desired neutron reaction $A + n \rightarrow C^*$ is substituted by a surrogate reaction $B + b \rightarrow C^* + c$ that forms the same compound nucleus, C^* (assumed to be a compound nuclear state in statistical equilibrium). The fission decay probability of C^* is then found by measuring the number of CN events that decay by fission, $N_{(b,cf)}$, relative to the total number of CN events measured in the experiment, $N_{(b,c)}$, according to

$$G_f^{\mathrm{CN}}(E_n) = \frac{N_{(b,cf)}(E_n)}{\epsilon_f N_{(b,c)}(E_n)} \equiv \frac{N_{(b,cf)}(E_n)}{\epsilon_f \epsilon_c \rho_T \ell_t Q \sigma_c}, \qquad (2)$$

where ϵ_f and ϵ_c are the fission and particle detection efficiencies, ρ_T is the areal target density, ℓ_t is the experimental live time, Q is the integrated charge delivered by the beam, and σ_c is the cross section for forming the CN in the surrogate reaction.

The (n,f) cross section of interest can subsequently be deduced from the fission decay probability measured in the surrogate experiment and a calculated neutron formation cross section, σ_n, via the equation

$$\sigma_{(n,f)}(E_n) = \sigma_n^{\mathrm{CN}}(E_n) G_f^{\mathrm{CN}}(E_n). \qquad (3)$$

If contaminants are present in a target, measuring the total number of CN events becomes experimentally challenging, and even small amounts of contamination in the target (e.g., carbon and oxygen) can lead to large errors in the deduced (n,f) cross sections. The surrogate ratio method (SRM) [4,5] removes the necessity to measure the total number of CN events in the experiment and therefore avoids several possible sources of significant systematic errors including contaminant contributions. In the SRM, two surrogate measurements, X and Y, are performed using an identical experimental setup but with different targets. In this case, the detection efficiencies (both ϵ_f and ϵ_c) cancel and the ratio of the surrogate formation cross sections, σ_c, is assumed to be unity, so that the only terms that remain from the denominator on the right-hand side of Eq. (2) are ρ_T, ℓ_t, and Q. The ratio of the fission cross sections can then be written as

$$\frac{\sigma^X_{(n,f)}(E_n)}{\sigma^Y_{(n,f)}(E_n)} = \frac{\sigma_n^{\mathrm{CNX}}(E_n)}{\sigma_n^{\mathrm{CNY}}(E_n)} \frac{(\rho_T \ell_t Q)^Y}{(\rho_T \ell_t Q)^X} \frac{N^X_{(b,cf)}(E_n)}{N^Y_{(b,cf)}(E_n)}, \qquad (4)$$

where the second term on the right-hand side is the correction factor between the two experiments, which is independent of energy. The values of σ_n^{CNX} and σ_n^{CNY} can be calculated within an optical model while $N^X_{(b,cf)}(E_n)/N^Y_{(b,cf)}(E_n)$ is measured directly in the surrogate experiment by counting light ions observed in prompt coincidence with fission fragments from two different target species. Typically, either $\sigma^X_{(n,f)}(E_n)$ or $\sigma^Y_{(n,f)}(E_n)$ is well established so that the other can be deduced from the surrogate ratio.

III. EXPERIMENTAL PROCEDURE

Two targets of ^{239}Pu and ^{235}U were used for the surrogate experiment. The target thicknesses were measured by α counting where the respective half lives are 2.4×10^4 years

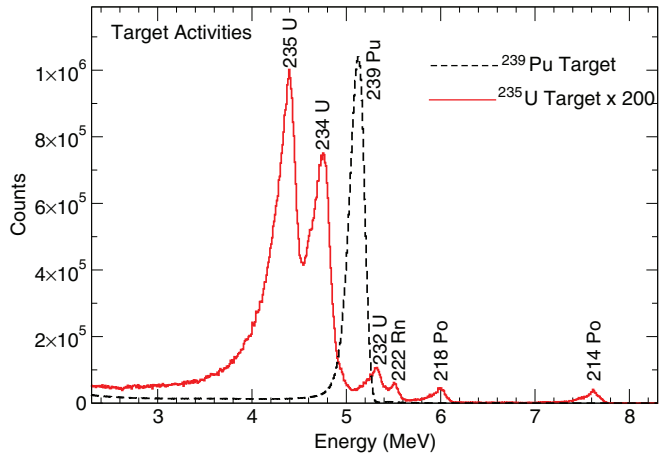

FIG. 2. (Color online) Activity spectra for the ^{235}U (solid line) and ^{239}Pu (dotted line) targets. The ^{235}U counts have been multiplied by 200 to provide similar scales. For the ^{235}U target, background lines from the ^{226}Ra decay chain are visible as well as trace isotopic contaminants of ^{232}U and ^{234}U.

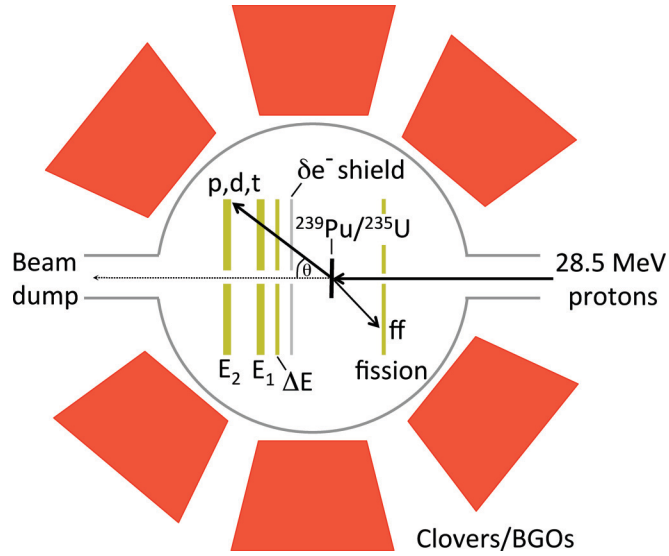

FIG. 3. (Color online) The STARLiTeR array at Texas A&M. The particle array consists of a position-sensitive silicon telescope at forward angles for light ion detection and a fission fragment detector at backward angles. Up to six compton-suppressed clover γ-ray detectors surround the target chamber.

and 7×10^8 years for ^{239}Pu and ^{235}U. The ^{239}Pu target was counted for 1 hour while the longer lived ^{235}U target was counted for 66 hours. This method is insensitive to the carbon backing and potential contaminant species in either target. Figure 2 presents the activity spectra for ^{239}Pu and ^{235}U. For both targets, contaminant isotopic species are less than 1%; however, in the case of the ^{235}U, the long half-life means that a prominent ^{234}U line and small ^{232}U line are apparent in the alpha spectrum as well as contaminant lines from the ^{226}Ra decay chain (which was used as a calibration source). Despite the comparable sizes of the ^{235}U and ^{234}U α peaks, the much shorter lived ^{234}U ($T_{1/2} = 2.5 \times 10^5$ years) constitutes less than a 0.03 % contaminant. A ^{235}U/^{239}Pu target thickness ratio, independent of the detector efficiency, was deduced to be 2.58(18) from the spectra in Fig. 2, after correcting for run length, live time, and half lives. The uncertainty primarily originates from separating the ^{235}U and ^{234}U α peaks.

A beam of 28.5-MeV protons from the K-150 cyclotron facility at Texas A&M University was used to bombard the ^{239}Pu and ^{235}U targets, as well as calibration targets of ^{12}C and ^{208}Pb at the target position of the STARLiTeR array. Data were collected for 66.3 hours on the ^{239}Pu target with an average proton beam intensity of 1.45(2) enA and an average live time of 74.9(1) %. For ^{235}U, the measurement time was 30.0 hours with an average intensity of 1.56(2) enA and an average live time of 74.6(1) %.

STARLiTeR comprises the Silicon Telescope Array for Reaction Studies (STARS) and the Livermore-Texas-Richmond array (LiTeR) of up to six Compton-suppressed clover γ-ray detectors (five were used in the present experiment). The setup is shown in Fig. 3. For the present experiment, STARS consisted of one 140 μm (ΔE) and two 1000 μm ($E1$ and $E2$) Micron S2 type silicon detectors placed downstream of the target for the detection of outgoing protons, deuterons and tritons between 36° and 67° with respect to the beam. Another 140 μm Micron S2 type detector was placed upstream for the detection of coincident fission fragments at backward angles between ~108° and 135°. Each S2 detector had 8 sectors and 24 1-mm-wide rings to provide position sensitivity in measuring incident charged particles. The target position was placed 15 mm from the front face of the ΔE detector. A 4 mg/cm^2 Al δ-electron shield was placed between the target and the ΔE detector to stop forward-going fission fragments and δ electrons produced in the target.

During the experiment, coincident signals in the ΔE and $E1$ detectors were required for a valid light-ion particle event to be recorded. Individual signals collected in the ΔE, $E1$, $E2$, fission, and γ-ray detectors had both energy and timing information on an event-by-event basis, so that prompt particle-γ and particle-fission coincidence events could be reconstructed from the data. In the energy range relevant to the (p,df) and (p, tf) reactions, all particles were stopped in the $E1$ detector. However, the $E2$ detector was needed for stopping protons and higher energy deuterons.

In order to discriminate between outgoing protons, deuterons and tritons, the empirical range-energy equation for silicon [30] is used:

$$\frac{T}{a} = \cos\theta[(E + \Delta E)^{1.7} - E^{1.7}], \qquad (5)$$

where T is the thickness of the ΔE detector; a is a constant for a given ion that relates its energy and range; θ is the incident angle of the particle and the power 1.7 relates to the stopping power of silicon. Figure 4 presents a plot of T/a versus ion energy for outgoing light ions in coincidence with fission fragments for the ^{235}U target data. The different bands representing protons, deuterons, and tritons are well separated in the present experiment.

Figure 5 shows fission fragments measured in coincidence with deuterons for both target datasets. The fission spectra

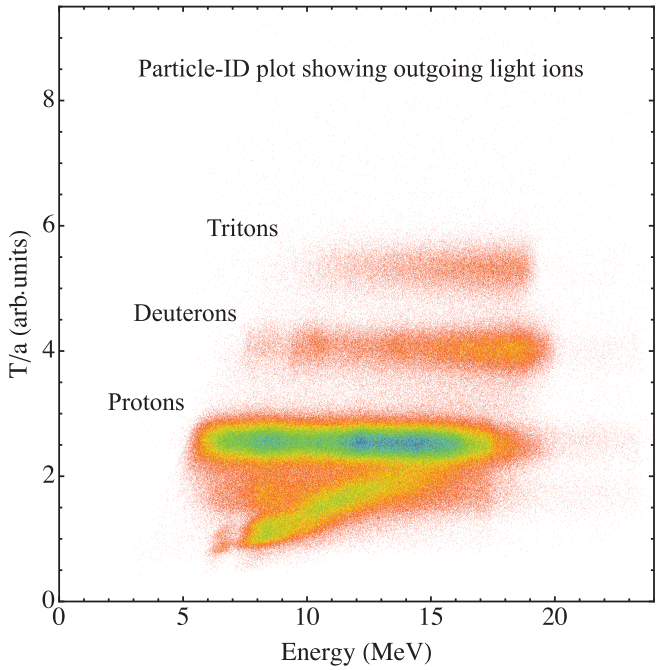

FIG. 4. (Color online) Linearized particle-identification plot showing outgoing protons, deuterons, and tritons observed in coincidence with fission in the STARS Si telescope for a proton beam incident on ^{235}U. The diagonal line of protons represents high-energy ions punching through all detector elements. The protons, deuterons, and tritons are clearly separated.

associated with tritons were observed to be similar. The spectrum for the thicker ^{235}U target is pushed to lower energies and broadened, presumably due to more energy straggling of the fission fragments as they traverse the target.

The measured charged particle energies are converted into CN excitation energies and subsequently into equivalent

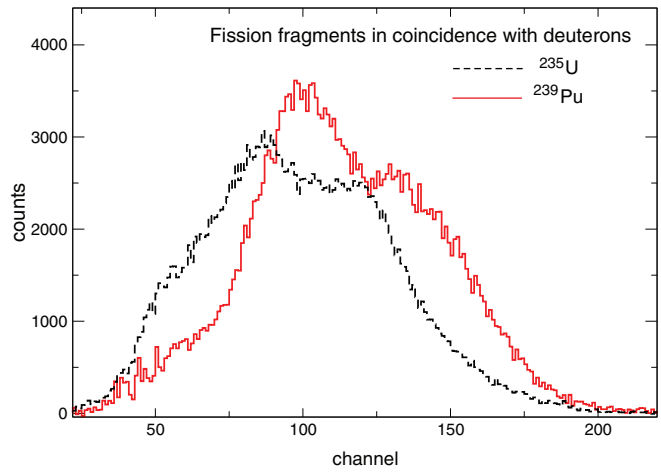

FIG. 5. (Color online) Fission spectra obtained in coincidence with deuterons measured in the ^{239}Pu$(p,df)^{238}$Pu and ^{235}U$(p,df)^{234}$U reactions. The fission spectrum associated with ^{235}U$(p,df)^{234}$U is pushed to lower energies and is broadened due to the ^{235}U target being thicker than the ^{239}Pu target.

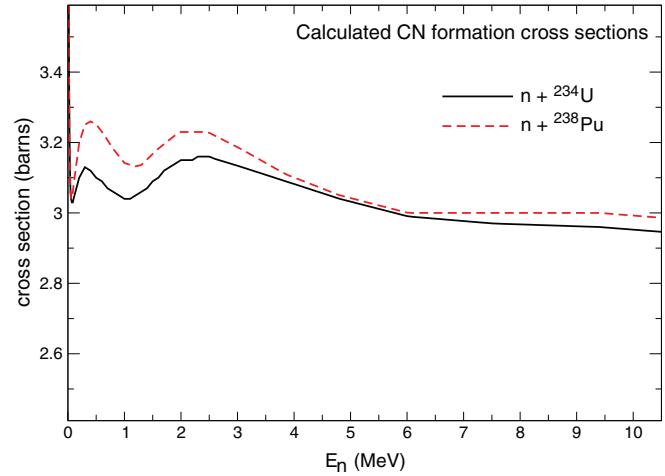

FIG. 6. (Color online) Calculated CN formation cross sections for $n+^{238}$Pu and $n+^{234}$U.

neutron energies, E_n. This is achieved by correcting for the recoil energy imparted to the CN, the energy losses of the charged particle as it traverses the δ-electron shield and detector dead layers (using the code ELAST [31]), and the reaction Q value. The energy scale is then set to be at $E_n = 0$ MeV coinciding with the CN neutron separation energy, S_n, for each surrogate reaction.

A. Compound nucleus formation cross sections

In the present work, CN formation cross sections, $\sigma_n^{\mathrm{CN}}(E_n)$, were calculated for ^{238}Pu and ^{234}U using the coupled-channels code ECIS [32] with the Soukhovitskii optical potential [33]. These formation cross sections, shown in Fig. 6, provide the $\sigma_n^{\mathrm{CN\,Pu}}(E_n)/\sigma_n^{\mathrm{CN\,U}}(E_n)$ ratio in Eq. (4) when deducing the (n,f) cross sections from the surrogate data. Since the CN formation cross sections vary slowly between isotopes, they can be used for all three surrogate measurements discussed below.

For the optical model calculations, the number of rotational states was varied to ensure convergence, and the deformation parameters were varied in order to estimate uncertainties. Uncertainties for the individual cross sections are about 1.5% (above 2 MeV). For the cross section ratio, the uncertainties are uncorrelated and can be added quadratically. Taking into account possible small errors due to the choice of the optical potential, the overall uncertainty is estimated to be about 3%, for neutron energies above about 2 MeV. Below 2 MeV, the optical model is known to be less accurate, so the estimated uncertainty in the ratio of the CN formation cross sections is 10%.

B. Relative corrections and uncertainties

The relative correction between the Pu and U target datasets [cf. Eq. (4)] is found to be $\frac{(\rho_T \ell_t Q)^{235\mathrm{U}}}{(\rho_T \ell_t Q)^{239\mathrm{Pu}}} = 0.80(7)$. The systematic error in this value originates from uncertainties in the live time (1%), integrated beam on target (2%), beam position variation with time on the inhomogenous targets (4%) and target thickness ratio (7%) for the ^{235}U and ^{239}Pu datasets.

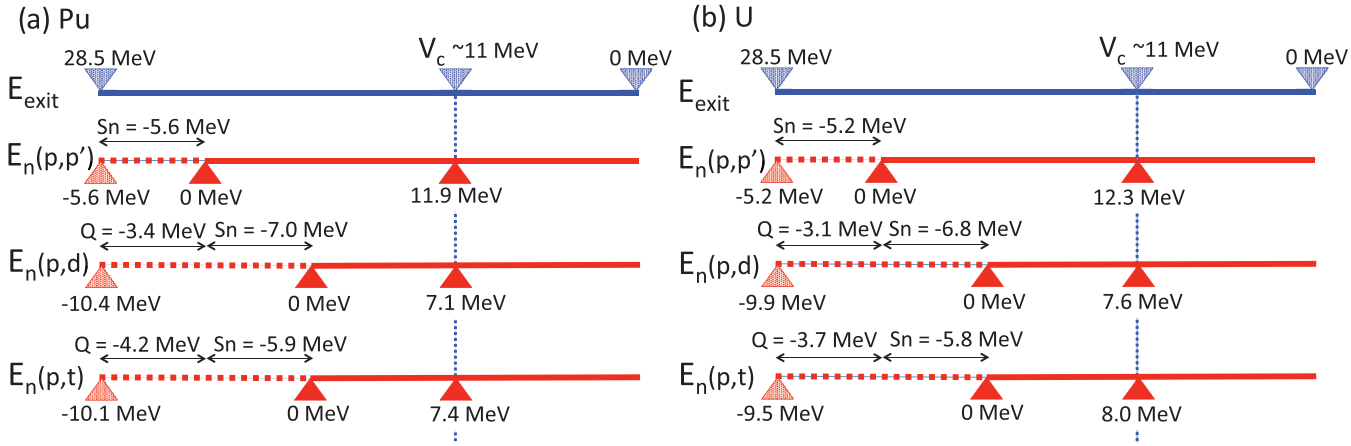

FIG. 7. (Color online) Comparison of outgoing beam-like particle energies ($E_{\rm exit}$) to equivalent neutron energies for (p,p'), (p,d), and (p,t) reactions on (a) ^{239}Pu and (b) ^{235}U. E_n is obtained by shifting the various reaction channels for the appropriate Q values and neutron separation energies. Smaller corrections for particle energy losses in dead layers and recoil corrections are accounted for in the analysis but omitted in the figure for clarity.

Uncertainties in the deduced cross sections are comprised of statistical errors from the particle-fission data, a systematic error introduced by the correction factor between the two data sets, as well as an additional 3% error above 2 MeV and 10% error below 2 MeV due to the uncertainty in the calculated $\sigma_n^{\rm CN\,Pu}(E_n)/\sigma_n^{\rm CN\,U}(E_n)$ ratio previously discussed.

The distribution of fission fragments with respect to the recoiling nucleus is anisotropic [34] and can also potentially introduce an energy-dependent uncertainty to the present results. As was the case in Refs. [16,19], it was found in the present work that such effects were negligible within the experimental uncertainties of the surrogate ratio data.

The uncertainty in particle energies can be measured by fitting discrete population peaks in particle spectra obtained by requiring specific γ-ray coincidences in the particle-γ coincidence data. The energy uncertainties of discrete states in ^{207}Pb, ^{233}U, and ^{238}Pu were studied and were typically observed to have 70–80 keV 1σ widths. A conservative energy uncertainty of 100 keV is thus assumed for the equivalent neutron energies in the surrogate data. This uncertainty can be ascribed to energy straggle of outgoing light ions in the target and detection system, angular detection resolution, intrinsic detector resolution and cyclotron beam energy resolution.

Figure 7 clarifies the relationship between the various energies used in this work. The energies of the outgoing beam-like particles, which lie between 28.5 and 0 MeV, are compared to the equivalent neutron energies of the CN populated in the (p,p'), (p,d), and (p,t) reaction channels for (a) Pu and (b) U targets. For (p,p') reactions the particle energy is corrected for only S_n, while for the (p,d) and (p,t) reaction channels the energies are shifted to account for the reaction Q value and S_n value in each case [35]. For clarity, energy losses and recoil corrections are not shown in Fig. 7. The Coulomb barrier is estimated to be $\sim$11.0 MeV [36] for these $Z = 1$ light-ion reactions on $Z \sim 90$ targets. The approximate E_n values where the outgoing light ion energy falls below this are indicated in the figure. It has previously been observed [19] that surrogate measurements deviate from the directly measured (n,f) cross section at equivalent neutron energies above this region due to the energies of the corresponding outgoing light ions falling below the nominal Coulomb barrier. The effective energy range for each surrogate reaction thus lies between the two filled triangles in Fig. 7 [i.e., between equivalent neutron energies of about 0–12 MeV for the (p,p') reaction, 0–7 MeV for the (p,d) reaction, and 0–7.5 MeV for the (p,t) reaction]. It should also be kept in mind that the spin transfer mismatch between the neutron-induced and surrogate reaction can lead to neutron cross sections deduced via surrogate measurements being unreliable below about 1 MeV [5].

IV. RESULTS AND DISCUSSION

A. Deducing the ^{237}Pu(n,f) cross section via the (p,d) surrogate ratio

Particle spectra for deuterons in coincidence with fission fragments for the ^{239}Pu(p,df) (dotted line) and ^{235}U(p,df) (solid line) data are given in Fig. 8. The data have been corrected to account for the different integrated beams, target thicknesses, and live times in the Pu and U datasets [cf. Eq. (4)]. The data are compressed to 100 keV/channel and the energy scales are given in equivalent neutron energies after allowing for the neutron separation energies of 7.0 and 6.8 MeV, respectively, for the ^{238}Pu and ^{234}U CN formed in the (p,d) reactions.

The ratio of the U and Pu data is presented in Fig. 9(a) (data points). For comparison, the ratio of the ENDF/B-VII $\sigma(^{233}{\rm U}(n,f))/\sigma(^{237}{\rm Pu}(n,f))$ data [22] are shown by the broken line. The dotted vertical line at 7 MeV indicates the approximate energy above which the data become unreliable. As discussed above, this energy (and above) corresponds to the deuteron energies falling below the nominal Coulomb barrier.

Figue 9(b) compares the extracted ^{237}Pu(n,f) cross section, from the surrogate ratio in (a) and the ENDF/B-VII ^{233}U(n,f) cross section (points with error bars), to the ENDF/B-VII [22] evaluated $\sigma(^{237}{\rm Pu}(n,f))$ data. The present result agrees with the ENDF evaluation. When compared to the earlier surrogate

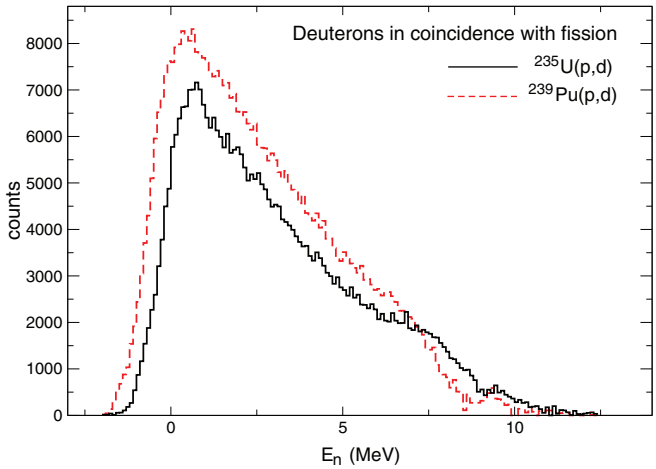

FIG. 8. (Color online) Deuterons in coincidence with fission for the ^{235}U(p,df) (solid line) and ^{239}Pu(p,df) (dotted line) reactions.

work shown in Fig. 1(a), the present results agree with those of Britt and Wilhelmy [20]. The results are also consistent with Younes *et al.* [21] down to ∼1 MeV. Below 1 MeV, the results differ from those of Younes *et al.* by as much as 1 barn. We attribute this large difference to residual spin-parity mismatch effects between the surrogate and neutron-induced reactions. Britt and Wilhelmy ignored the effect in their analysis, while Younes *et al.* used reaction modeling to correct for the mismatch. Their model did, however, not include the possibility of projectile breakup for the ^{3}He beam, so the treatment could be further improved. The present work makes use of the surrogate ratio approach, which has been shown to mitigate, but not correct for, the spin-parity mismatch. The remaining differences between the three results indicate that further work is required to properly account for the spin-mismatch effect at low neutron energies (below ∼1 MeV) and potentially also at the onset of second-chance fission [5].

B. The ^{236}Pu(n,f) cross section deduced utilizing the (p,t) surrogate ratio

The particle spectra for ^{239}Pu(p, tf) (dotted line) and ^{235}U(p, tf) (solid line) are presented in Fig. 10. Both spectra are compressed to 100 keV/channel while the U data is corrected relative to the Pu data to be consistent with equation 4. The neutron separation energies for ^{237}Pu and ^{233}U are 5.9 and 5.8 MeV, respectively, and the energy spectra in Fig. 10 are adjusted so that the equivalent neutron energy, E_n is zero at these respective energies.

The ratio of the U and Pu data is compared to the ENDF/B-VII evaluated ^{232}U(n,f)/^{236}Pu(n,f) cross section ratio in Fig. 11(a). Figure 11(b) presents the deduced ^{236}Pu(n,f) cross section (points with error bars) which utilizes the surrogate ratio from Fig. 11(a) and the ENDF/B-VII evaluation for $\sigma(^{232}\mathrm{U}(n,f))$. Figure 11(b) also shows a dashed line representing the $\sigma(^{236}\mathrm{Pu}(n,f))$ data from the ENDF/B-VII evaluation that is based upon data from Refs. [20,26,27]. Above ∼1.5 MeV the evaluation is consistently low relative to the surrogate data. It should be noted that the surrogate results of Britt and Wilhelmy [20] (see Fig. 1) also appear to be high with respect to the ENDF/B-VII evaluation, albeit their data still lie at ∼3 barns below 1.5 MeV.

C. The ^{238}Pu(n,f) cross section via the (p,p') surrogate ratio

The ^{238}Pu(n,f) cross section has previously been measured up to $E_n = 15$ MeV in a number of direct measurements as well as a recent (α,α') surrogate reaction [16]. The ENDF/B-VII and other evaluations for $\sigma(^{238}\mathrm{Pu}(n,f))$ are thus based upon more substantial experimental data than those for the ^{236}Pu(n,f) and ^{237}Pu(n,f) cross sections discussed above.

The higher energy inelastic protons are not all stopped in the STARS detectors. However, across the angular range of 45°–52°, inelastic protons within the energy range relevant for fission were all stopped in the $E1$ and $E2$ detectors. It was thus possible to deduce the ^{238}Pu(n,f) cross section from the

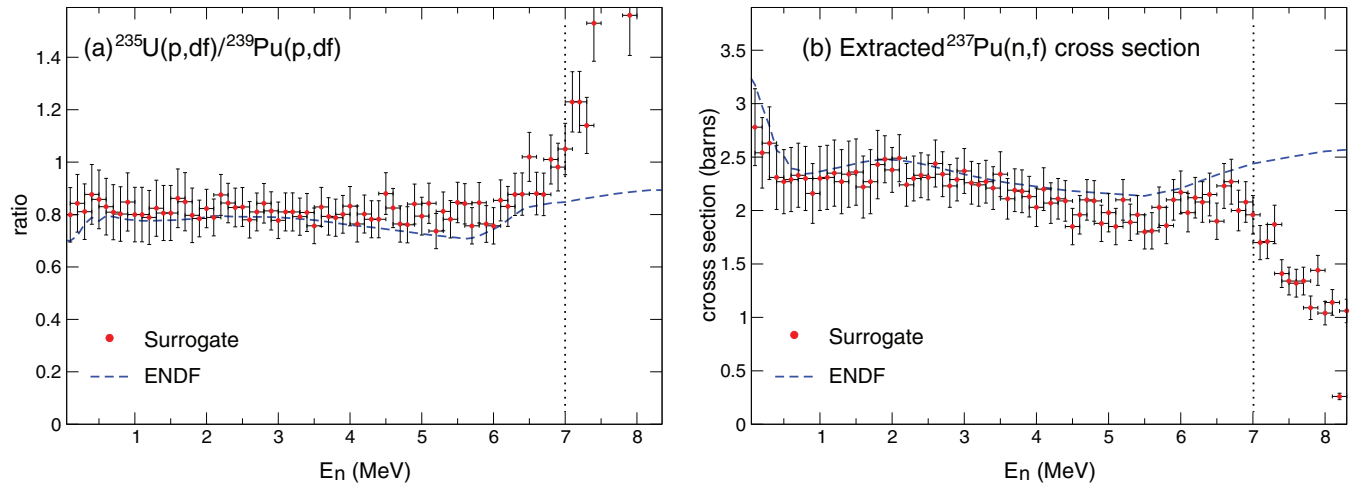

FIG. 9. (Color online) (a) The $\sigma(^{233}\mathrm{U}(n,f))/\sigma(^{237}\mathrm{Pu}(n,f))$ ratio determined from the ^{235}U(p,df) and ^{239}Pu(p,df) surrogate measurements (data points) and compared to the ENDF/B-VII value for the ratio (dashed line). (b) The data points show the ^{237}Pu(n,f) cross section extracted from the surrogate ratio in (a) and the ENDF/B-VII ^{233}U(n,f) cross section. The broken line represents the ENDF/B-VII evaluated ^{237}Pu(n,f) cross section. The error bars include statistical and systematic uncertainties as well as uncertainties introduced by the CN formation cross section calculations (cf. Sec. III B). Experimental data above the vertical dotted line at ∼7 MeV are considered unreliable (see text).

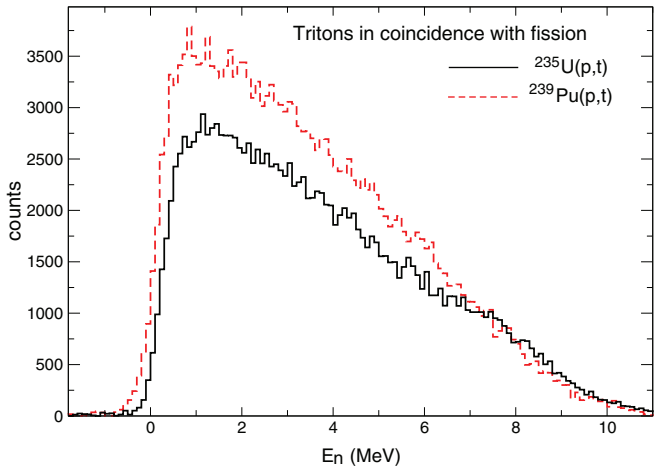

FIG. 10. (Color online) Comparison of triton spectra for the ^{235}U$(p,\ tf)$ and ^{239}Pu$(p,\ tf)$ reactions. The U data have been normalized to correct for the different integrated beam and target thicknesses in the two experiments.

^{235}U(p,p')/^{239}Pu(p,p') surrogate ratio measurement utilizing protons detected in this narrow angular range.

In the case of the (p,p') surrogate data, there is a 0.4 MeV relative shift between the ^{239}Pu and ^{235}U target data when correcting the proton energies to equivalent neutron energies (cf. Fig. 7). This shift means that the proton energies associated with a specific E_n value for the ^{239}Pu target fall below the Coulomb barrier sooner than protons corresponding to the same E_n value for the ^{235}U target. The shift has the effect of amplifiying the distortion caused by the Coulomb barrier. To address this issue for the (p,p') surrogate data, rather than shifting the surrogate data for the ^{239}Pu and ^{235}U targets, the 0.4 MeV relative shift is instead applied between the ^{234}U(n,f) and ^{238}Pu(n,f) ENDF/B-VII data. In this case, the same shift must also be applied to the CN formation cross section calculations. The cross section obtained by applying the energy shift to the ENDF/B-VII data is consistent with the cross section deduced by applying the energy shift to the surrogate data. The exceptions to this are below ~0.5 MeV, where the shift in the CN formation cross section calculations has a large effect, and also above 10.5 MeV where the impact of the Coulomb barrier distortion is lessened.

Figure 12 presents the ^{238}Pu(n,f) cross section deduced from the surrogate ratio and $\sigma(^{234}$U$(n,f))$ ENDF/B-VII evaluation (data points) and compares it to the ENDF/B-VII evaluated ^{238}Pu(n,f) cross section (solid line), as well as the (α,α') surrogate work of Ressler *et al.* [16]. There is relatively good agreement between the evaluated data and the present surrogate work above ~0.5 MeV and up to ~10.5 MeV. The present results are also consistent with the previous surrogate work of Ressler *et al.*, albeit their data appear to show a higher cross section near the second-chance fission threshold (~5–6 MeV) than the present work and the ENDF evaluation. It is possible this difference is related to the spin-mismatch between the different surrogate reactions which is expected to play a more substantial role near the threshold of first and second chance fission. The surrogate data from the present work are slightly lower than the ENDF evaluation betwen 10.5 and 12 MeV, while above ~12 MeV the data should be considered unreliable as suggested in Fig. 7.

The agreement between the surrogate and evaluated ^{238}Pu(n,f) cross section in the energy range $E_n = 0.5$–10.5 MeV gives an indication of the reliability of the surrogate ratio approach employed here not not just for the (p,p') surrogate data but also the (p,d) and (p,t) surrogate data discussed above. In particular, the relative correction of 0.80(7) utilized in Eq. (4) between the Pu and U target data is the same for the (p,p'), (p,d), and (p,t) reaction channels.

Figure 12 shows that the ^{238}Pu(n,f) data exhibit a maximum fission cross section of about 3 barns in the range $E_n \sim 7$–10 MeV, while the ^{236}Pu(n,f) data in Fig. 11(b) suggest a fission cross section of up to 3 barns in the range

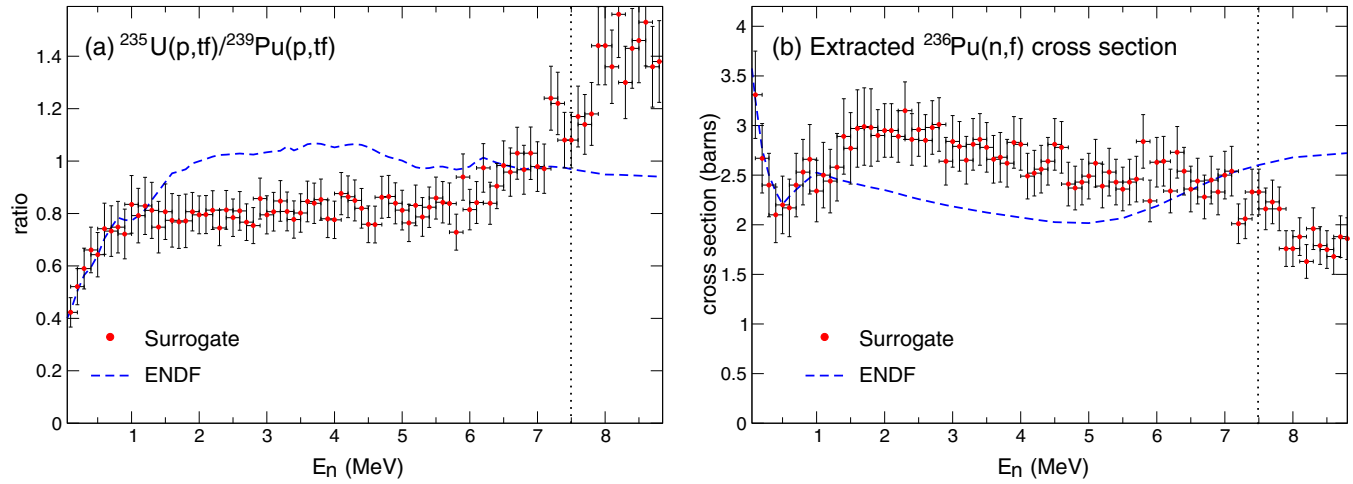

FIG. 11. (Color online) (a) The $\sigma(^{232}$U$(n,f))/\sigma(^{236}$Pu$(n,f))$ ratio as determined from the ^{235}U$(p,\ tf)$ and ^{239}Pu$(p,\ tf)$ surrogate measurements (data points) and compared to the ENDF/B-VII ratio (dotted line). (b) The ^{235}U(n,f) cross section extracted from the ratio in (a) and the ENDF/B-VII ^{232}U(n,f) cross section as compared to the ENDF/B-VII $\sigma(^{236}$Pu$(n,f))$ evaluation. The error bars include statistical and systematic uncertainties as well as uncertainties introduced by the CN formation cross section calculations (cf. Sec. III B). The extracted cross section data beyond the dotted vertical line at ~7.5 MeV are distorted as described in the text.

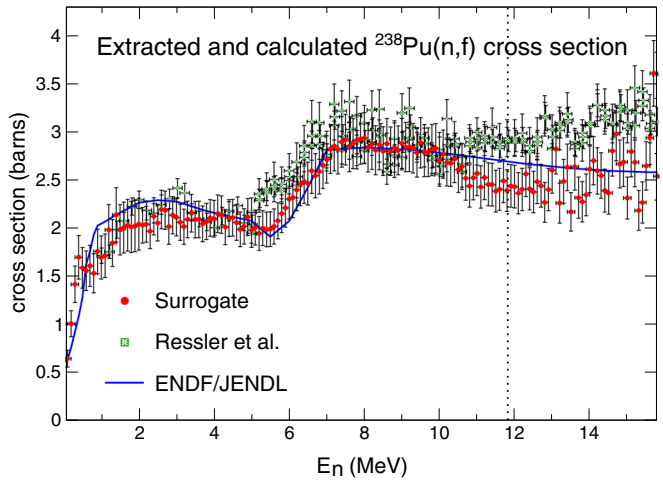

FIG. 12. (Color online) The ^{238}Pu(n,f) cross section deduced from the surrogate ratio and $\sigma(^{234}\mathrm{U}(n,f))$ ENDF/B-VII evaluation (solid circles), from prior surrogate work by Ressler *et al.* [16] (dotted squares) and from the ENDF/B-VII evaluation (solid line). The error bars in the present data include statistical and systematic uncertainties as well as uncertainties introduced by the CN formation cross section calculations (cf. Sec. III B), while the data above the vertical dotted line at ∼12 MeV are considered unreliable (see text).

$E_n \sim$ 2–7 MeV. However, Fig. 6 indicates that the total CN formation cross section for these isotopes should lie just above 3 barns in the energy range $E_n =$ 0–10 MeV. The present results therefore suggest that, at these energies, fission is the strongly dominant CN decay mechanism.

V. SUMMARY

Neutron-induced fission cross sections for the short-lived actinide nuclei, ^{236}Pu and ^{237}Pu have been deduced by utilizing the surrogate ratio method. The $\sigma(^{233}\mathrm{U}(n,f))/\sigma(^{237}\mathrm{Pu}(n,f))$ ratio was measured via (p,d) reactions on ^{235}U and ^{239}Pu targets and the $\sigma(^{232}\mathrm{U}(n,f))/\sigma(^{236}\mathrm{Pu}(n,f))$ ratio was determined via (p,t) reactions on the same targets. The ^{236}Pu(n,f) and ^{237}Pu(n,f) cross sections were subsequently deduced across respective equivalent neutron energy ranges of $E_n =$ 0.5–7 MeV and $E_n =$ 0.5–7.5 MeV. The $\sigma(^{237}\mathrm{Pu}(n,f))$ deduced in the present work is consistent with the ENDF/B-VII evaluation that utilized previous surrogate data. The deduced $\sigma(^{236}\mathrm{Pu}(n,f))$ suggests a cross section of up to 3 barns, higher than various nuclear data evaluations between 1.5 and 7 MeV, and the evaluated nuclear data for this isotope should be revisited.

Surrogate data for the (p,p') reaction channel on the ^{235}U and ^{239}Pu targets was also available so that the $\sigma(^{238}\mathrm{Pu}(n,f))$ cross section could be deduced. In this case the surrogate data agree with the well established ENDF/B-VII evaluation between 0.5 and 10.5 MeV.

The ^{236}Pu(n,f) and ^{238}Pu(n,f) cross sections show maximum values of about 3 barns in the ranges 2–7 MeV and 7–10 MeV, respectively. Calculated total compound nucleus formation cross sections suggests that this is close to the upper limit for the compound nucleus formation cross section. The results therefore imply that the fission channel strongly dominates the decay of the ^{237}Pu and ^{239}Pu compound nuclei at these energies.

ACKNOWLEDGMENTS

The authors are grateful for the efforts of the Texas A&M Cyclotron Institute's operations and facilities staff. This work was performed under the auspices of the US Department of Energy under Contracts No. DE-FG02-05 ER41379 and No. DE-FG52-06 NA26206 (University of Richmond), No. DE-AC52-07NA27344 and the Department of Energy's NNSA Office of Defense Nuclear Nonproliferation Research and Development (LLNL), and No. DE-FG52-09NA29467 from NNSA and No. DE-FG02-93ER40773 from the DOE Office of Nuclear Physics (TAMU).

[1] J. D. Cramer and H. C. Britt, Nucl. Sci. Eng. **41**, 177 (1970).
[2] J. D. Cramer and H. C. Britt, Phys. Rev. C **2**, 2350 (1970).
[3] M. Petit *et al.*, Nucl. Phys. A **735**, 345 (2004).
[4] C. Plettner *et al.*, Phys. Rev. C **71**, 051602(R) (2005).
[5] J. E. Escher and F. S. Dietrich, Phys. Rev. C **74**, 054601 (2006).
[6] J. T. Harke *et al.*, Phys. Rev. C **73**, 054604 (2006).
[7] B. F. Lyles *et al.*, Phys. Rev. C **76**, 014606 (2007).
[8] B. K. Nayak *et al.*, Phys. Rev. C **78**, 061602 (2008).
[9] S. R. Lesher *et al.*, Phys. Rev. C **79**, 044609 (2009).
[10] M. S. Basunia *et al.*, Nucl. Instrum. Methods B **267**, 1899 (2009).
[11] J. M. Allmond *et al.*, Phys. Rev. C **79**, 054610 (2009).
[12] B. L. Goldblum *et al.*, Phys. Rev. C **80**, 044610 (2009).
[13] J. T. Burke *et al.*, AIP Conf. Proc. **1005**, 96 (2008).
[14] G. Kessedjian *et al.*, Phys. Lett. B **692**, 297 (2010).
[15] R. Hatarik *et al.*, Phys. Rev. C **81**, 011602(R) (2010).
[16] J. J. Ressler *et al.*, Phys. Rev. C **83**, 054610 (2011).
[17] J. E. Escher, J. T. Harke, F. S. Dietrich, N. D. Scielzo, I. J. Thompson, and W. Younes, Rev. Mod. Phys. **84**, 353 (2012).
[18] A. Czeszumska *et al.*, Phys. Rev. C **87**, 034613 (2013).
[19] R. O. Hughes *et al.*, Phys. Rev. C **85**, 024613 (2012).
[20] H. C. Britt and J. B. Wilhelmy, Nucl. Sci. Eng. **72**, 222 (1979).
[21] W. Younes, H. C. Britt, and J. A. Becker, Tech. Rep. UCRL-TR-201913, LLNL (2004), doi:10.2172/15013937.
[22] M. B. Chadwick, M. Herman, P. Obložinský *et al.*, Nucl. Data Sheets **112**, 2887 (2011).
[23] K. Shibata *et al.*, J. Nucl. Sci. Technol. **39**, 1125 (2002).
[24] M. N. Nikolaev, Russian File of Evaluated Neutron Data, 2010, http://www.ippe.ru/podr/abbn/english/libr/rosfond.php
[25] Chen Guo-Chang *et al.*, Chin. Phys. C **36**, 823 (2012).
[26] P. E. Vorotnikov *et al.*, in *Proceedings of the First International Conference on Neutron Physics, Kiev, September 14–18, 1987* (TsNIIatominform, Moscow, 1988), Vol. 4, p. 76.
[27] E. A. Gromova *et al.*, At. Energ. **68**, 223 (1990).
[28] W. Hauser and H. Feshbach, Phys. Rev. **87**, 366 (1952).
[29] V. F. Weisskopf and D. H. Ewing, Phys. Rev. **57**, 472 (1940).
[30] F. S. Goulding, D. A. Landis, J. Cerny, and R. H. Pehl, Nucl. Instrum. Methods **31**, 1 (1964).

[31] Energy Loss and Straggle Tool [adapted from ENELOSS, written by H. Ernst (1981) and modified by K. Lesko (1984)].
[32] J. Raynal, computer code ECIS03, Nuclear Energy Agency Package ID NEA 0850/16, 2004 (unpublished).
[33] E. Sh. Soukhovitskii, R. Capote, J. M. Quesada, and S. Chiba, Phys. Rev. C **72**, 024604 (2005).
[34] R. Vandenbosch and J. R. Huizenga, *Nuclear Fission* (Academic, New York, 1973).
[35] G. Audi, A. H. Wapstra, and C. Thibault, Nucl. Phys. A **729**, 22 337 (2003).
[36] R. Bass, *Nuclear Reactions with Heavy Ions* (Springer-Verlag, New York, 1980), pp. 318–340.